ResearchGate

See discussions, stats, and author profiles for this publication at: https://www.researchgate.net/publication/231209692

Three-Dimensional Structure and Subunit Topology of the V1 ATPase from Manduca sexta Midgut†

ARTICLE *in* BIOCHEMISTRY · JULY 2000

Impact Factor: 3.02 · DOI: 10.1021/bi000103u

CITATIONS
67

READS
22

9 AUTHORS, INCLUDING:

Jasminka Godovac Zimmermann
University College London
124 PUBLICATIONS **3,360** CITATIONS
SEE PROFILE

Benito Cañas
Complutense University of Madrid
74 PUBLICATIONS **2,694** CITATIONS
SEE PROFILE

Markus Huss
Universität Osnabrück
44 PUBLICATIONS **1,228** CITATIONS
SEE PROFILE

William R Harvey
University of Florida
120 PUBLICATIONS **4,164** CITATIONS
SEE PROFILE

Available from: Markus Huss
Retrieved on: 01 February 2016

Three-Dimensional Structure and Subunit Topology of the V_1 ATPase from *Manduca sexta* Midgut[†]

Gerhard Grüber,*[,‡,§] Michael Radermacher,[||] Teresa Ruiz,[||] Jasminka Godovac-Zimmermann,[⊥] Benito Canas,[⊥] Daniela Kleine-Kohlbrecher,[‡] Markus Huss,[‡] William R. Harvey,[§] and Helmut Wieczorek[‡]

Universität Osnabrück, Fachbereich Biologie/Chemie, D-49069 Osnabrück, Germany, Whitney Laboratory, University of Florida, St. Augustine, Florida 32086, Max-Planck-Institut für Biophysik, Abteilung Strukturbiologie, D-60528 Frankfurt am Main, Germany, and University College London, Centre for Molecular Medicine, London WC1E 6JJ, United Kingdom

Received January 19, 2000; Revised Manuscript Received March 22, 2000

ABSTRACT: The three-dimensional structure of the *Manduca sexta* midgut V_1 ATPase has been determined at 3.2 nm resolution from electron micrographs of negatively stained specimens. The V_1 complex has a barrel-like structure 11 nm in height and 13.5 nm in diameter. It is hexagonal in the top view, whereas in the side view, the six large subunits A and B are interdigitated for most of their length (9 nm). The topology and importance of the individual subunits of the V_1 complex have been explored by protease digestion, resistance to chaotropic agents, MALDI-TOF mass spectrometry, and $CuCl_2$-induced disulfide formation. Treatment of V_1 with trypsin or chaotropic iodide resulted in a rapid cleavage or release of subunit D from the enzyme, indicating that this subunit is exposed in the complex. Trypsin cleavage of V_1 decreased the ATPase activity with a time course that was in line with the cleavage of subunits B, C, G, and F. When $CuCl_2$ was added to V_1 in the presence of CaADP, the cross-linked products A−E−F and B−H were generated. In experiments where $CuCl_2$ was added after preincubation of CaATP, the cross-linked products E−F and E−G were formed. These changes in cross-linking of subunit E to near-neighbor subunits support the hypothesis that these are nucleotide-dependent conformational changes of the E subunit.

V- and F-ATPases consist of a mosaic of globular structural units, including domain and secondary structures, which also serve as functional units. These ATPases belong to two related families of ion pumps which are thought to use a common mechanism to couple the energy of ATP hydrolysis to ion transport and thus create an electrochemical gradient across the membrane. V- and F-ATPases are characterized by a membrane-embedded, ion-conducting complex, V_O or F_O, and an extrinsic complex, V_1 or F_1, in which ATP hydrolysis takes place (*1*−*3*). Whereas the major V-ATPase subunits A and B appear to be homologous to the F-ATPase subunits β and α, respectively, it is difficult to identify V_1 subunits that have any similarity to the smaller polypetides of F_1. The smaller V_1 subunits C−H are described as stalk subunits (*4*) and are thought to provide the structural and physical coupling between the catalytic sites and the ion-conducting complex.

The V_1 ATPase from tobacco hornworm, *Manduca sexta*, which is made up of the eight different subunits A−H with apparent molecular masses of 67, 56, 54, 40, 32, 28, 16, and 14 kDa (*5*, *6*), is the object of these studies. The enzyme, as shown by small-angle X-ray scattering data, is highly elongated with a maximal length of about 22 nm. It has a radius of gyration, R_g, of 6.1 nm and a molecular mass of 550 kDa. The solution scattering data define a complex with a headpiece approximately 14.5 nm in diameter and a stalk approximately 11 nm in length, perpendicular to the headpiece (*7*). More recently, we used electron microscopy as a tool complementary to X-ray small-angle scattering and obtained two-dimensional average images of this V_1 ATPase in negative stain (*8*). These images reveal a pseudohexagonal arrangement of six masses, interpreted as three copies each of the major subunits A and B, surrounding a central cavity containing a seventh mass. Here, we used tilt pairs of negatively stained preparations to determine the first three-dimensional reconstruction of the V_1 ATPase at a resolution of 3.2 nm. Our results add to the emerging picture of V_1 in which three copies of the A and B subunits are arranged as a hexagonal barrel, interdigitated for much of their length and enclosing a cavity of approximately 3.5 nm. This three-dimensional model allows a comparison with structural models of the closely related F_1 ATPase determined by electron microscopy (*9*) and X-ray crystallography (*10*−*14*).

Further insights into the topology of the V_1 ATPase and the role of constituent subunits were obtained by protease

[†] This research was supported by the Deutsche Forschungsgemeinschaft (Wi698 and SFB 431), Welcome Trust Grant 054096, Special Trustees of the Middlesex and University College Hospitals G.83, National Institutes of Health Grant A1 22444, and NSF Grant DBI-9515518.

* To whom correspondence should be addressed at Universität Osnabrück, Fachbereich Biologie/Chemie, D-49069 Osnabrück, Germany. Phone: +49/(0)541 969 3504; Fax: +49/(0)541 969 3503; E-mail: ggrueber@biologie.uni-osnabrueck.de.

[‡] Universität Osnabrück.

[§] University of Florida.

[||] Max-Planck-Institut für Biophysik.

[⊥] University College London.

10.1021/bi000103u CCC: $19.00 © 2000 American Chemical Society
Published on Web 07/18/2000

digestion of the V_1 complex. The rates of cleavage of individual subunits of V_1 are discussed in terms of their function. Responses of individual subunits to treatment with chaotropic iodide were used as a measure of the stability of their integration into the complex. Finally, $CuCl_2$-induced cross-link formation between various subunits of V_1 was used to examine subunit−subunit interactions of the enzyme as a function of nucleotide binding.

MATERIALS AND METHODS

Materials. Chemicals for gel electrophoresis were obtained from Serva (Heidelberg). All other chemicals were at least of analytical grade and obtained from Merck (Darmstadt), Sigma (Deisenhofen), or Serva (Heidelberg). Trypsin used for in-gel digestion was obtained from Promega (Madison, WI).

Purification of the V_1 ATPase. Tobacco hornworms were reared as reported previously (*15*). The V_1 ATPase from *M. sexta* midgut was isolated according to Gräf et al. (*16*) and Merzendorfer et al. (*17*). Protein concentrations were determined with Amido Black (*18*). SDS[1]−polyacrylamide gel electrophoresis was performed with 17.5% total acrylamide and 0.4% cross-linked acrylamide. Protein bands on gels were stained with Coomassie Brilliant Blue R (*15*). ATPase activity was measured as described previously (*16*, *18*).

Electron Microscopy and Image Processing. For electron microscopy, the protein was diluted to a final concentration of 0.05 mg/mL by 20 mM Tris-HCl (pH 8.1) and 50 mM NaCl. The sample was applied to 400 mesh copper grids using the carbon sandwich technique (*19*) with 0.5% uranyl acetate as a negative stain. Each micrograph was recorded at an instrumental magnification of 59200× at 100 kV using an electron dose of approximately 10 e^- per Å^2. The experiments were performed on a Philips CM 120 electron microscope. The three-dimensional reconstruction followed the random conical reconstruction technique of Radermacher et al. (*20*) and Radermacher (*21*) as implemented in the SPIDER software package (*22*). Six pairs of micrographs, the first image in each pair recorded at 50° and the second at 0° tilt angle, were scanned on a flat-bed SCAI (Zeiss) microdensitometer with 7 μm pixel size, which was subsequently reduced by binning to a pixel size of 21 μm. A total of 1407 pairs of images of single V_1 ATPases were selected. The criteria used for this selection were that the V_1 molecules should be clearly visible and separated from neighboring particles in both the tilted and untilted versions, and that they should appear in the hexagonal orientation, the most common view, in the 0° image. The images of untilted V_1 particles were translationally and rotationally aligned by correlation methods [e.g., (*23*)] and submitted to correspondence analysis (*23*−*25*) and classification (*26*). A total of 1384 images were used in the final reconstruction. For representation, the reconstruction was low-pass-filtered to 3.0 nm.

Trypsin Digestion Studies. V_1 ATPase was incubated at a concentration of 8 mg/mL with trypsin in a ratio of 1:250 (w/w) in 20 mM Tris-HCl (pH 8.0), 30 mM NaCl, and 4 mM EDTA at 30 °C. Trypsin cleavage was stopped by addition of soybean trypsin inhibitor in a ratio to trypsin of 4:1 (w/w), and aliquots were withdrawn for measurements of ATPase activity and for gel electrophoresis. After staining (Coomassie Brilliant Blue R), the relative stain intensities of the bands were determined using the program Quantity One-4.0.3 (Fluor-S MultiImager, BIORAD).

In-Gel Tryptic Protein Digestion and Mass Spectrometric Analysis. The cleavage fragments, called B′ and B″, were cut out from the SDS−polyacrylamide gel and destained with a solution of 25 mM ammonium bicarbonate and 50% acetonitrile for 12 h. Gel bands were cut into small pieces of 1 mm^3, washed 3 times with acetonitrile, dried for 30 min in a speed-vacuum concentrator, and digested according to a procedure modified from Hellmann et al. (*27*) and Roos (*28*).

For MALDI mass spectrometry, aliquots of 0.5 μL of the digested solution were applied to a target disk and allowed to air-dry. Subsequently, 0.5 μL of matrix solution (1% w/v α-cyano-4-hydroxycinnamic acid in 50% acetonitrile, 0.1% v/v trifluoroacetic acid) was applied to the dried sample and again allowed to dry. Spectra were obtained using a Bruker Biflex III MALDI-TOF mass spectrometer. For the identification of the protein fragments, the MASCOT program available at the Matrixscience web site (http://www.matrixscience.com) was used.

Influence of Chaotropic Iodide. The V_1 complex was incubated in a solution consisting of 0.8 M KI, 150 mM NaCl, 20 mM Tris-HCl, and 9.6 mM 2-mercaptoethanol at a pH of 8.1 for 45 min on ice. Afterward the mixture was loaded onto a Superdex 200 HR 10/30 column (Pharmacia) equilibrated with the same buffer as above but without KI, and subjected to gel permeation chromatography (FPLC) at a flow rate of 0.5 mL/min.

$CuCl_2$-Induced Cross-Link Formation. The enzyme solution as isolated contained 9.6 mM 2-mercaptoethanol. To remove 2-mercaptoethanol and loosely bound nucleotides, the sample was passed through a Superdex 200 HR 10/30 gel chromatography column (Pharmacia), equilibrated in 20 mM Tris-HCl (pH 8.1) and 150 mM NaCl. An absorbance ratio of enzyme to nucleotide (A_{280}/A_{260}) greater than 1.6 was found after the column step. Cross-linking was induced by incubation with 100 μM $CuCl_2$ in a buffer containing 20 mM Tris-HCl (pH 8.1) and 150 mM NaCl for 1 h on ice. The cross-linking reaction was stopped by addition of 7.5 mM EDTA. For the analysis of cross-linked products, samples were dissolved in DTT-free dissociation buffer and applied to an SDS−polyacrylamide gel as described above.

RESULTS

Electron Microscopy and Three-Dimensional Reconstruction. Electron micrographs of the same field of negatively stained V_1 ATPase, isolated from the larval *Manduca sexta* midgut, taken at tilt angles of 0° and 50° are shown in Figure 1A,B. Images from six tilted/untilted pairs of micrographs were selected, aligned, classified, and used for the three-dimensional reconstruction. A two-dimensional average from the 0° micrographs of the particles that were used for the three-dimensional reconstruction shows all of the detailed features of the hexagonal arrangement of the major subunits A and B (Figure 2). The final three-dimensional reconstruc-

[1] Abbreviations: AMP·PNP, 5′-adenylyl imidodiphosphate; DTT, dithiothreitol; EDTA, ethylenediaminetetraacetic acid; KI, potassium iodide; MALDI, matrix-assisted laser desorption ionization; NEM, *N*-ethylmaleimide; PAGE, polyacrylamide gel electrophoresis; SDS, sodium dodecyl sulfate.

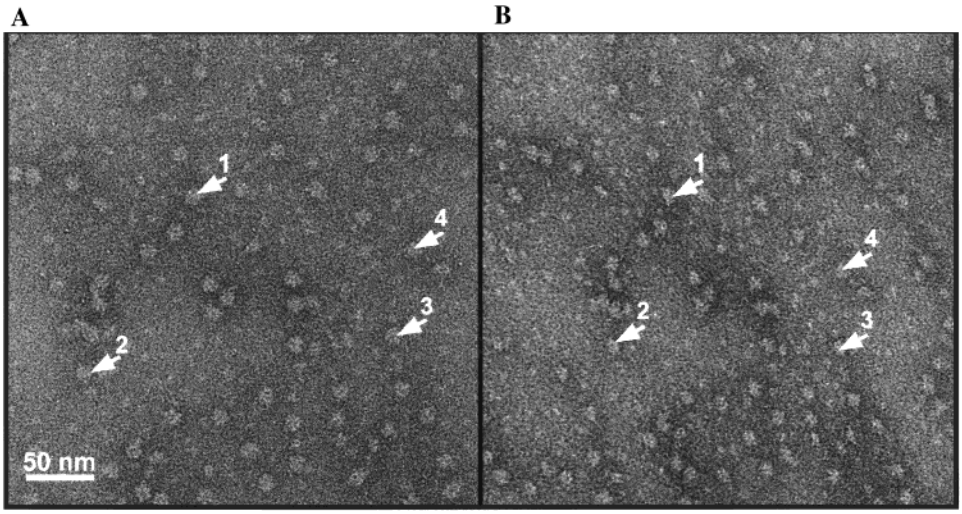

FIGURE 1: Electron micrographs of negatively stained V_1 ATPase from *Manduca sexta* at tilt angles of 0° (A) and 50° (B). Bar represents 50 nm.

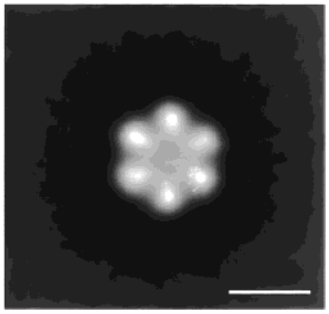

FIGURE 2: Average of 1384 images at 0° used to compute the three-dimensional reconstruction. Bar represents 10 nm.

tion (Figure 3) is based on 1384 images and showed a resolution of 3.2 nm, as determined by the Fourier shell correlation (FSC_5) criterion (*21, 29*) with a threshold of 5 times the noise correlation value. Using Radermacher's formula (*21, 30*), the resolution in the direction of the missing cone (the *z*-direction) is 1.48 times the resolution in the $x-y$ plane (47 Å). The double layer negative staining technique with uranyl acetate was used to avoid artifacts caused by only partial staining of the specimen, which in turn would lead to inconsistent projections for a three-dimensional reconstruction. However, the drying artifacts which occur in the staining procedure are orientation dependent (*31*) and in most cases do not allow the combination of data from particles in different orientation. Thus, angular reconstitution techniques could not be used to fill the missing cone. Indeed, when applied to images from other specimens stained with uranyl acetate, as was done here, angular reconstitution has led to entirely artifactual results (unpublished results).

One of the main striking features of the reconstruction is the presence of six elongated lobes, approximately 2 nm in diameter and approximately 9 nm in length, which are parallel to the 3-fold axis (Figure 3, panels A and D). These lobes, presumably representing the alternating three copies each of subunits A and B, can be traced for most of the length of the V_1 ATPase. The hexagonal barrel of subunits A and B encloses a core approximately 3.5 nm in diameter (Figures 2 and 3). The model of the V_1 complex has a barrel-like shape that is approximately 11 nm high and 13.5 nm across. The stalk, which can be seen in two-dimensional averages of the V_1V_O ATPase from *Clostridium fervidus* (*32*−*34*) and from bovine clathrin-coated vesicles (*35*), is not obvious in our reconstruction. The lack of visibility of the stalk can be attributed to drying artifacts that occurred during the preparation of the specimen. However, at both ends of the hexagonal barrel, extensions can be observed. The extensions on one side can be attributed to traces of the stalk, most probably the entire asymmetric mass visible in Figure 3, panels A−C. The extensions on the opposite side are consistent with published two-dimensional average images of the V_1V_O ATPase, where elongated features in a *crown*-like fashion can be seen at the very top of the V_1 domain (*33*−*35*).

The three-dimensional reconstruction was calculated only for the native V_1 complex. A two-dimensional analysis of trypsinized V_1 ATPase (see below) revealed quite a significant variation among particles (not shown), from which we concluded that the structural variations are too large for three-dimensional difference imaging. In many experiments where portions are deleted, structural variations extend through the whole molecule (*56*), preventing three-dimensional difference imaging to be used for localization of deleted portions of the protein.

Trypsin Treatment of the V_1 ATPase. To examine the topology of the stalk subunits (C−H), not resolved in the three-dimensional reconstruction described above, as well as the functional importance of individual subunits of the V_1 complex, we have used the approaches of protease digestion, MALDI-TOF mass spectrometry, dissociation by chaotropic agents, and cross-linking experiments. The time course of proteolysis was probed by SDS/PAGE, in which the trypsin-treated samples were compared with a control sample of untreated V_1 ATPase (Figure 4A). The B subunit was cleaved rapidly, and two new fragments, with apparent molecular masses of 25 and 34 kDa, B′ and B″, respectively, were generated. With longer incubation times (up to 25 min), subunit B was cleaved further, thereby increasing the amount of B′ (64% of subunit B) and B″ (15% of subunit B). Both fragments were subjected to in-gel tryptic digestion. MALDI mass spectrometry was used for the analysis of the entire mixture of the tryptic peptides. A Mascot software package was used to identify the subunit fragments that were

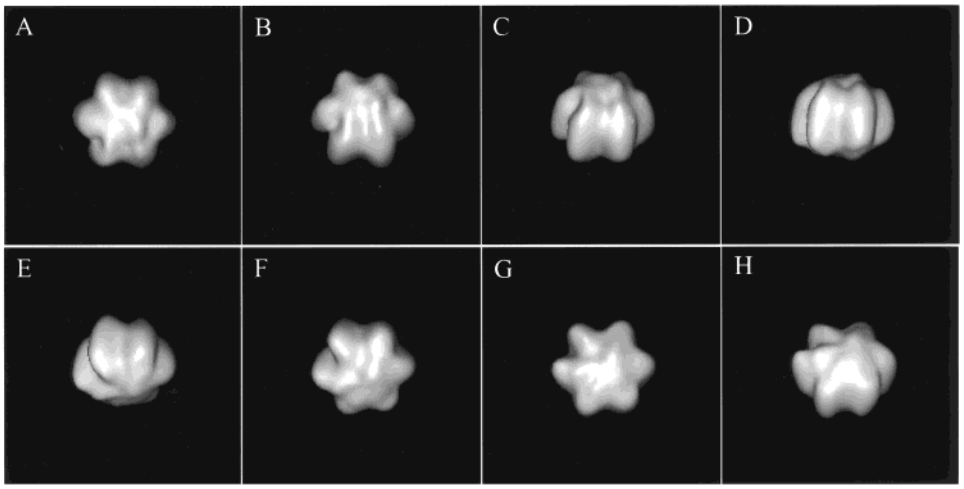

FIGURE 3: Surface representation of the three-dimensional reconstruction of the V_1 ATPase. The particle is represented as rotating around an axis parallel to the specimen support. The structure is formed by the A_3B_3 hexamer and protrusions visible on either surface of the hexamer. The protrusion observed in panels A−C is most probably an indication of the stalk connecting to the V_O part of the V_1V_O ATPase.

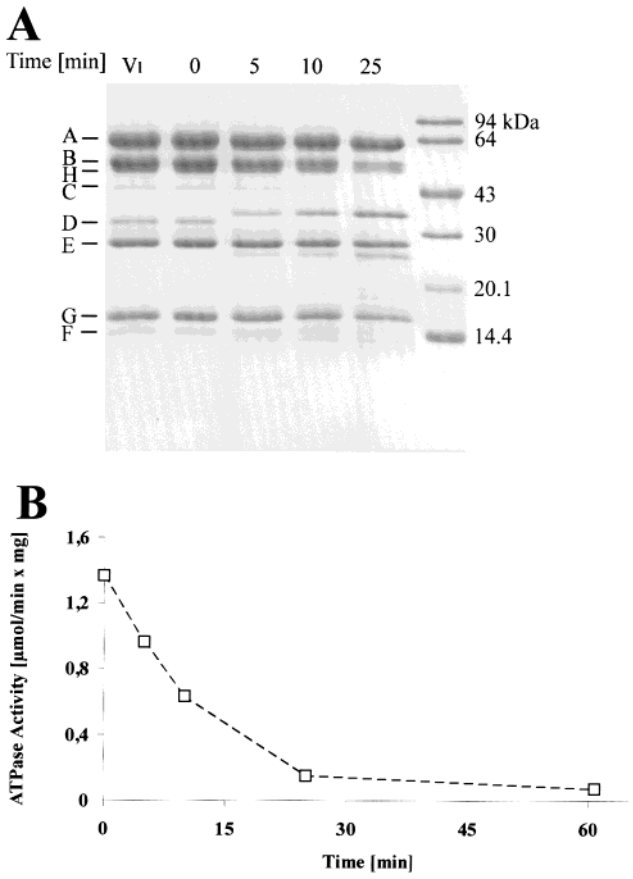

FIGURE 4: Time course of trypsin cleavage of V_1 ATPase from *M. sexta* (A). V_1 ATPase (8 μg) was incubated with trypsin [250:1 (w/w)] for the indicated time before the reaction was stopped by addition of soybean trypsin inhibitor. Samples were electrophoresed on a 17.5% total acrylamide and 0.4% cross-linked acrylamide gel. (B) Effect of proteolysis on the enzyme activity of the V_1 ATPase.

consistent with the observed peptide masses obtained by MALDI-TOF mass spectrometry (spectra not shown). Both B′ and B″ were identified as bands deriving from subunit B. The former contained the amino acids after Arg_{305}, and the latter consisted of the peptide Met_1-Arg_{191} (*36*). The sequence $I_{146}-R_{168}$ of fragment B″ (Table 1) is interesting because either none, one, or both of the two containing Met residues were oxidized in a ratio of 0.9:1.1:1.0, respectively. Whether this finding, which cannot be caused by treatment during mass spectrometry, reflects an intrinsic asymmetry of the three B subunits in a V_1 complex cannot be analyzed at this stage.

Among the *stalk* subunits, C−H, subunit D was cleaved most rapidly by trypsin, followed by the F, G, C, and H subunits, with the E subunit being the most slowly modified. Cleavage of the D subunit did not produce any major fragments that could be detected in the staining profile, implying that this subunit was digested to small peptides not detectable in the electrophoresis procedure.

ATPase activity of the V_1 complex was examined during trypsinolysis. The time course of decrease in ATP hydrolysis (Figure 4B) corresponded to the cleavage of subunits B, C, G, and F, and the increase of the resulting fragments B′ and B″, but was not affected by the rapid cleavage of subunit D. The enzyme became 90% inhibited with the accessibility for trypsin to subunits A, E, and H.

Treatment of the V_1 Complex with Chaotropic Iodide. Chaotropic agents, such as iodide, tend to make water more disordered and lipophilic and thus may weaken hydrophobic interactions (*37*). Treatment of the V_1 ATPase with chaotropic iodide therefore should primarily and most rapidly affect those subunits in the complex which (i) mainly interact with other subunits by way of hydrophobic interactions and (ii) are not shielded by other subunits and thus are free to dissociate from the complex. Chaotropic agents are well-known to cause removal of V_1 subunits from the membrane-bound V_O complex (*1*) and, at higher concentrations, to cause V_1 disintegration into subcomplexes and monomers (*38*). To determine which subunits are exposed in the molecule and therefore most sensitive to treatment with iodide, the V_1 ATPase was incubated for 45 min on ice with 0.8 M potassium iodide and then subjected to gel permeation chromatography. Two main peaks, which both lacked subunits D and F, were obtained (Figure 5). The higher molecular mass peak additionally lacked most of subunit A, whereas the lower molecular mass peak appeared to have lost subunit C and part of subunit H in addition to subunits D and F. Both fractions had also lost all enzyme activity.

Table 1: MALDI Mass Spectrometry Analysis of the B″ Fragment

start residue	end residue	expected mass	measured mass	delta mass	sequence[a]
59	65	768.65	769.66	0.27	LADGHTR
21	27	861.61	862.62	0.18	DFISQPR
13	20	909.63	910.64	0.12	EHVLAVSR
51	58	962.62	963.63	0.08	FSEIVQLK
104	113	1103.60	1104.61	0.07	TPVSEDMLGR
104	113	1119.58	1120.59	0.06	TPVSEDMLGR[b]
92	103	1451.81	1452.82	0.10	NTLCEFTGDILR
77	91	1519.85	1520.86	0.07	AVVQVFEGTSGIDAK
32	47	1638.99	1639.99	0.07	TVSGVNGPLVILDEVK
4	20	1794.07	1795.08	0.10	TLSAAQANKEHVLAVSR
32	50	2011.26	2012.27	0.13	TVSGVNGPLVILDEVKFPK
172	191	2191.30	2192.30	0.14	IPIFSAAGLPHNEIAAQICR
147	168	2450.35	2451.36	0.13	IYPEEMIQTGISAIDVMNSIAR
125	146	2462.36	2463.36	0.10	GPPILAEDFLDIQGQPINPWSR
147	168	2466.35	2467.35	0.13	IYPEEMIQTGISAIDVMNSIAR[b]
147	168	2482.35	2483.36	0.14	IYPEEMIQTGISAIDVMNSIAR[c]

[a] 13 peptides cover 83.2% (159/191 amino acids). [b] One oxidized methionine. [c] Two oxidized methionines.

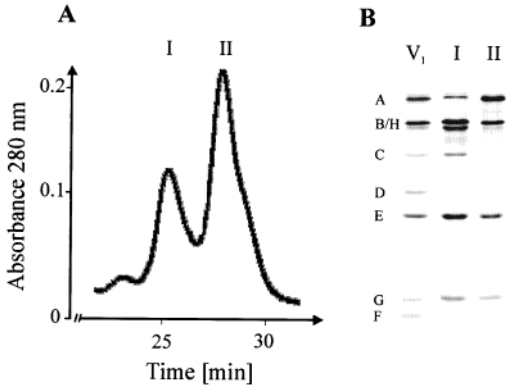

FIGURE 5: Influence of chaotropic potassium iodide on the stability of the V_1 complex. (A) Elution profile after FPLC using a Superdex 200 column. I and II indicate the two main peaks visualized at 280 nm. (B) SDS−polyacrylamide electrophoresis of V_1 ATPase before treatment with iodide (V_1) and of aliquots taken from fractions I and II obtained after chromatography of the iodide-treated sample. Silver stains (*55*) with 1 μg of protein per lane.

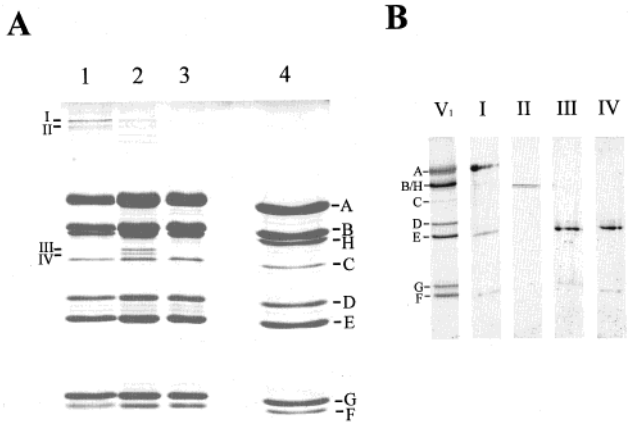

FIGURE 6: Nucleotide-dependent disulfide bond formation in the V_1 ATP of *M. sexta*. (A) Before electrophoresis the enzyme was incubated with 100 μM $CuCl_2$ in the presence of 2 mM CaADP (lane 1) or 2 mM Ca ATP (lane 2) and in the absence of nucleotides (lane 3), as described under Materials and Methods. A control without $CuCl_2$ is shown in lane 4. The gel was stained with Coomassie Blue. (B) The cross-linked products I, II, III, and IV in the gel from panel A were cut out, destained, soaked in buffer consisting of 20 mM Tris-HCl (pH 8.1), 50 mM DTT, and 0.5% SDS, and placed onto a 17.5% total acrylamide and 0.4% cross-linked acrylamide gel. The gel was stained with silver.

Cross-Linking of V_1 Subunits Induced by $CuCl_2$ Treatment. For a disulfide bond to be formed, two cysteine residues must have their α-carbon atoms within 4−9 Å of each other (*39*). This fact was used to examine the proximity of V_1 subunits to each other and their functional relationship by disulfide formation of endogenous cysteines in the enzyme complex. Disulfide formation was mediated by Cu^{2+}, which transiently binds to the thiol group. Figure 6A shows the results of cross-linking of the V_1 ATPase with $CuCl_2$ under different nucleotide conditions. When the enzyme was incubated with 2 mM CaADP on ice before Cu^{2+} treatment, two new bands with apparent molecular masses of 120 and 110 kDa were obtained (lane 1). In contrast, when cross-linking was conducted in 2 mM CaATP on ice to slow ATP hydrolysis and retain ATP in a catalytic site during the reaction (lane 2), two new bands with apparent molecular masses of 42 and 44 kDa were generated between the H and C subunits with only small amounts of 120 and 110 kDa species being formed. Cross-linked products similar to those shown in lane 2 were observed when the cross-linking reaction in the presence of CaATP was stopped after 5 min by the addition of 7.5 mM EDTA (not shown); these data ruled out that CaATP was converted into CaADP + P_i before cross-link formation and therefore establish that the differences in cross-linking pattern seen in comparing lanes 1 and 2 were due to a difference in whether CaADP or CaATP was bound in the nucleotide binding site of the V_1 ATPase. Disulfide bond formation could not be induced by $CuCl_2$ addition to the enzyme in the absence of nucleotides (lane 3). To analyze the new disulfide bond formations, the 42, 44, 110, and 120 kDa products were cut out from the gel, destained, and subjected to SDS−polyacrylamide gel electrophoresis in the presence of dithiothreitol (DTT). As shown in Figure 6B, the 120, 110, 44, and 42 kDa products contain subunits A−E−F (lane I), B−H (lane II), E−G (lane III), and E−F (lane IV), respectively.

DISCUSSION

The three-dimensional reconstruction of the V_1 ATPase from *M. sexta* determined from negatively stained specimens reveals a barrel-like structure with hexagonal modulations and dimensions of 13.5 nm in diameter and 11 nm in height (Figure 3). A hexagonal arrangement of densities identified

as subunits A and B has been seen in projection images of single V_1 molecules in stain [(*8*, *32*); see also Figure 2]. The studies presented here also confirmed the A_3, B_3 stoichiometry of the subunits. In three dimensions, these peripheral subunits are elongated structures, interdigitated for most of the height of the V_1 complex. Only near the ends of the complex does the 6-fold modulation disappear. The extension seen on both sides of the structure can be attributed to traces of the stalk on one side and to the *crown*-like feature observed in two-dimensional average images of the V_1V_O ATPase from *C. fervidus* (*32*−*34*) and bovine clathrin-coated vesicles (*35*). Such a structural extension is similar to the top domain of the quaternary structure of the V_1 complex from *M. sexta* that was determined from X-ray small-angle scattering data (*7*). By comparison, a *crown*-like feature has been obtained from crystallographic analysis of the closely related F_1 ATPases (*10*−*14*). The *crown* of the F_1 ATPases, made by a β-barrel domain, containing the N-termini of the major subunits α and β, is important for the stabilization (*10*, *11*) and assembly (*40*) of the molecule. It has been shown recently by three-dimensional reconstruction of the *Escherichia coli* F_1F_O ATPase from electron microscopic images that this *crown* changes its shape upon binding of the noncleavable nucleotide analogue AMP·PNP (*41*).

A two-dimensional analysis had shown that the A_3B_3-barrel of the V_1 ATPase from *M. sexta* is partly occluded by a seventh mass either centrally or asymmetrically to the hexamer (*8*). This hexagonal arrangement of the A_3B_3 subcomplex and an asymmetrically placed seventh mass is remarkably similar to the subunit arrangement of the F_1 complex. Cryo-electron micrographs of F_1 molecules from *E. coli* that were labeled with Fab fragments of monoclonal antibodies (*42*) or with monomaleimido gold (*43*, *44*) have shown that the additional off-centered mass includes the stalk subunits γ and ϵ.

Small-angle X-ray scattering data have yielded a model of the hydrated V_1 complex, consisting of a hexagonal headpiece 14.5 nm in diameter and 11 nm in height, which agrees with the hexagonal domain of the EM-based model, and a *stalk* of 11 nm in length (*7*). The stalk is not resolved in our three-dimensional reconstruction, presumably due to dehydration and adsorption of the V_1 particles to the carbon film. However, the shape and interdigitation of the A_3B_3 subunits, located around the periphery of the barrel, strongly resemble the three-dimensional models of the F_1 ATPase, obtained by cryo-microscopy (*42*) and X-ray crystallography (*10*, *12*−*14*), in which the alternating subunits α and β interdigitate for the full length surrounding the γ subunit.

Protease digestion data presented here (Figure 4) for the *M. sexta* V_1 ATPase and recent studies of the V-ATPase from *Saccharomyces cerevisiae* (*45*) show that subunit B is more susceptible to proteolysis than subunit A. The increase of the major cleavage product B′, including the C-terminal part in which nucleotide binding occurs, as shown by photoactivity labeling of 2-azido[^{32}P]ATP (*46*), is in line with the decrease of ATP hydrolysis. Trypsin treatment of the *S. cerevisiae* V-ATPase has demonstrated that the degradation of subunit B is accelerated in the presence of 5 mM MgATP (*45*). This finding implies that the B subunit undergoes significant conformational changes due to nucleotide binding. The effect of nucleotide-dependent conformational changes

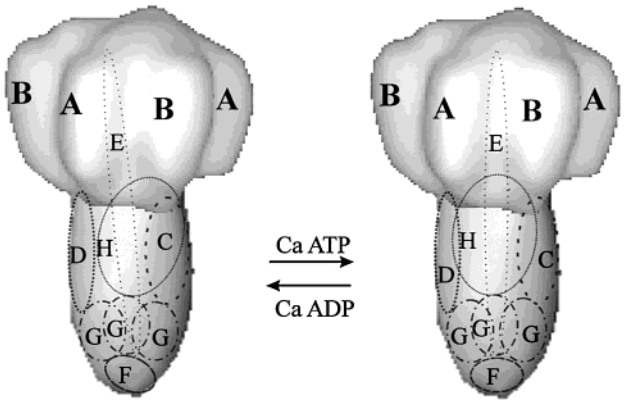

FIGURE 7: Model of the subunit arrangement in the V_1 ATPase from *M. sexta* and their nucleotide-dependent rearrangement based on the combination of the presented three-dimensional reconstruction and biochemical studies. The V_1 subunits (C−H) are placed within the shape of the stalk of the V_1 ATPase from *M. sexta* determined from solution X-ray scattering data (*7*). When Ca ADP is bound to the enzyme, the cross-links between A−E−F and B−H can be generated, whereas in the presence of CaATP the cross-link products E−G and E−F can be observed.

and the correlation between increase of fragment B′ with the decrease of ATP hydrolysis add evidence to support the hypothesis that the B subunit plays an important role in hydrolyzing ATP.

The accessibility of trypsin to subunits C, G, and F is consistent with the V_1 model, derived from the subcomplex assembly of yeast V_1 *stalk* subunits (*4*), in which the smaller peptides F and G, which seem to link the V_1 with the V_O portion, have been placed at the bottom of the *stalk* and subunit C at its periphery. The loss of subunit F upon treatment with chaotropic iodide reported here (Figure 5) is in accordance with this view as well as with the observation that subunit F reassociates with a V_1 complex devoid of F only when it is present in large excess (*16*). In the model of yeast V_1, subunit H has been located between an AB-interface and subunit C, and thus should be protected against rapid cleavage, as observed by trypsinolysis of the *M. sexta* V_1 complex. Our cross-linking data place the H subunit close to the B subunit (shown schematically in Figure 7).

An important finding is the slow cleavage of subunit E and the rapid cleavage of subunit D, both of which have been proposed as structural and functional homologues of the γ subunit of F-ATPases (*47*, *48*). The observation that the D subunit is cleaved immediately into small peptides by trypsin treatment is surprising and implies that this polypeptide is rather susceptible to trypsin (see Figure 7). Its release from the V_1 complex due to treatment with chaotropic iodide also allows the interpretation that this subunit is not shielded extensively by other subunits in the stalk. The opposite is true for subunit E, which is very resistant to chaotropic treatment. Subunit E becomes accessible to trypsin only after advanced cleavage of subunits B, C, F, and G. As shown by $CuCl_2$-induced disulfide formation (see above), subunit E binds to subunits F and G, when CaATP binds to the enzyme. A homologous cross-linked product consisting of subunits E and G has also been generated using dimethyl sulfoxide as an oxidant (*4*). The trypsin cleavage and the cross-linking data reported here imply that one region of subunit E is shielded by the smaller subunits F and G (see Figure 7). In

addition, the disulfide bond that forms between the catalytic A subunits and subunit E in the presence of CaADP indicates that these subunits are near neighbors. The close proximity of subunit E to both the catalytic subunit A and the subunits F and G would allow coupling of the catalytic site events in subunit A via the E subunit to the small subunits F and G, which are in close proximity to the proton-translocating V_O portion (*4*). Involvement of subunit E in coupling is also indicated by the cross-linked products A−E−F, when CaADP is bound, whereby E forms disulfide bonds with both subunits F and G in the presence of CaATP (see Figure 7).

Comparisons of the recently identified structures of the V_1 ATPase from *Clostridium fervidus* (*32*) and *M. sexta* (*7*) using electron microscopy and X-ray small-angle scattering, respectively, reveal a molecule with a pseudo-3-fold symmetry and a central *stalk* of significant length. Side view projections of the negatively stained V_1V_O ATPase from *C. fervidus* show a peripheral stalk of approximately 13 nm in length, proposed to be formed by the V_O portion and to function as a stator (*49*). The presence of a second stalk is also described in electron micrographs of the closely related F_1F_O ATPase from *E. coli* (*41, 50*), chloroplasts (*51*), and bovine heart mitochondria (*52*), keeping the $\alpha_3\beta_3$ hexamer fixed relative to the rotating parts. More recently, a second peripheral stalk has been described from negatively stained images of the V_1V_O ATPase from *C. fervidus* (*33, 34*) and from bovine clathrin-coated vesicles (*35*). The question that now arises is, which subunits of the V_1V_O ATPase may contribute to this putative second stator. Proposed candidates include subunits I, E, and F (*33*). Previous experiments on the interactions between different subunits (*4, 16, 53, 54*) and the results presented here suggest that subunits E and F contribute to the central stalk (see Figure 7).

REFERENCES

1. Stevens, T. H., and Forgac, M. (1997) *Annu. Rev. Cell Dev. Biol. 13*, 779−808.
2. Bowman B. J., and Bowman E. J. (1997) in *The Mycota III. Biochemistry And Molecular* Biology (Brambl and Marzluf, Eds.) pp 57−83.
3. Allison, W. S. (1998) *Acc. Chem. Res. 31*, 819−826.
4. Tomashek, J. J., Graham, L. A., Hutchins, M. U., Stevens, T. H., and Klionsky, D. J. (1997) *J. Biol. Chem. 272*, 26787−26793.
5. Wieczorek, H., Grüber, G., Harvey, W. R., Huss, M., and Merzendorfer, H. (1999) *J. Bioenerg. Biomembr. 31*, 67−74.
6. Huss, M., Grüber, G., Harvey, W. R., Merzendorfer, H., Schmid, R., and Wieczorek, H. (1999) *Zoology 102 (Suppl. II)*, 66.
7. Svergun, D. I., Konrad, S., Huss, M., Koch, M. H. J., Wieczorek, H., Altendorf, K., Volkov, V. V., and Grüber, G. (1998) *Biochemistry 37*, 17659−17663.
8. Radermacher, M., Ruiz, T., Harvey, W. R., Wieczorek, H., and Grüber, G. (1999) *FEBS Lett. 453*, 383−386.
9. Gogol, E. P., Lücken, U., Bork, T., and Capaldi, R. A. (1989) *Biochemistry 28*, 4709−4716.
10. Abrahams, J. P., Leslie, A. G. W., Lutter, R., and Walker, J. E. (1994) *Nature 370*, 621−628.
11. Shirakihara, Y., Leslie, A. G. W., Abrahams, J. P., Walker, J. E., Ueda, T., Sekimoto, Y., Kambara, M., Saika, K., Kagawa, Y., and Yoshida, M. (1997) *Structure 5*, 825−836.
12. Bianchet, M. A., Hullihen, J., Pedersen, P. L., and Amzel, M. L. (1998) *Proc. Natl. Acad. Sci. U.S.A. 95*, 11065−11070.
13. Hausrath, A. C., Grüber, G., Matthews, B. W., and Capaldi, R. A. (1999) *Proc. Natl. Acad. Sci. U.S.A. 96*, 13697−13702.
14. Stock, D., Leslie, A. G. W., and Walker, J. E. (1999) *Science 286*, 1700−1705.
15. Schweikl, H., Klein, U., Schindlbeck, M., and Wieczorek, H. (1989) *J. Biol. Chem. 264*, 11136−11142.
16. Gräf, R., Harvey, W. R., and Wieczorek, H. (1996) *J. Biol. Chem. 271*, 20908−20913.
17. Merzendorfer, H., Gräf, R., Huss, M., Harvey, W. R., and Wieczorek, H. (1997) *J. Exp. Biol. 200*, 225−235.
18. Wieczorek, H., Cioffi, M., Klein, U., Harvey, W. R., Schweikl, H., and Wolfersberger, M. G. (1990) *Methods Enzymol. 192*, 608−616.
19. Tischendorf, G. W., Zeichhardt, H., and Stöffler, G. (1974) *Mol. Gen. Genet. 134*, 187−208.
20. Radermacher, M., Wagenknecht, T., Verschoor, A., and Frank, J. (1987) *J. Microsc. 146*, 113−136.
21. Radermacher, M. (1988) *J. Electron Microsc. Tech. 9*, 359−394.
22. Frank, J., Smith, B., and Dowse, H. (1981) *Ultramicroscopy 6*, 343−358.
23. Frank, J., and Radermacher, M. (1992) *Ultramicroscopy 46*, 241−262.
24. van Heel, M., and Frank, J. (1981) *Ultramicroscopy 6*, 187−194.
25. Frank, J., and van Heel, M. (1982) *J. Mol. Biol. 161*, 134−137.
26. Frank, J., Bretaudiere, J. P., Carazo, J. M., Verschoor, T., and Wagenknecht, T. (1988) *J. Microsc. 150*, 99−115.
27. Hellman, U., Wernstedt, C., Gonez, J., and Heldin, C.-H. (1995) *Anal. Biochem. 224*, 451−455.
28. Roos, M., Soskic, V., Poznanovic, S., and Godovac-Zimmermann, J. (1998) *J. Biol. Chem. 273*, 924−931.
29. Saxton, W. O., and Baumeister, W. (1982) *J. Microsc. 127*, 127−138.
30. Radermacher, M., and Hoppe, W. (1980) *Proc. 7th Eur. Congr. Electron Microsc. 1 (The Hague)*, 132−133.
31. Carazo, J. M., Wagenknecht, T., and Frank. J. (1989) *Biophys. J. 55*, 465−477.
32. Boekema, E. J., Ubbink-Kok, T., Lolkema, J. S., Brisson, A., and Konings, W. N. (1998) *Photosynth. Res. 57*, 267−273.
33. Boekema, E. J., van Breemen, J. F. L., Brisson, A., Ubbink-Kok, T., Konings, W. N., and Lolkema, J. S. (1999) *Nature 401*, 37−38.
34. Ubbink-Kok, T., Boekema, E. J., van Breemen, J. F. L., Brisson, A., Konings, W. N., and Lolkema, J. S. (2000) *J. Mol. Biol. 296*, 311−321.
35. Wilkens, S., Vasilyeva, E., and Forgac, M. (1999) *J. Biol. Chem. 274*, 31804−31810.
36. Novak, F. J. S., Gräf, R., Waring, Wolfersberger, M. G., Wieczorek, H., and Harvey, W. R. (1992) *Biochim. Biophys. Acta 1132*, 67−71.
37. Hatefi, Y., and Hanstein, W. G. (1969) *Proc. Natl. Acad Sci. U.S.A 62*, 1129−1136.
38. Lepier, A., Gräf, R., Azuma, M., Merzendorfer, H., Harvey, W. R., and Wieczorek, H. (1996) *J. Biol. Chem. 271*, 8502−8508.
39. Creighton, T. E. (1984) *Methods Enzymol. 107*, 305−329.
40. Bakhtiari, N., Lai-Zhang, J., Yao, B., and Mueller, D. M. (1999) *J. Biol. Chem. 274*, 16363−16369.
41. Böttcher, B., Bertsche, I., Reuter, R., and Gräber, P. (2000) *J. Mol. Biol. 296*, 449−457.
42. Gogol, E. P., Aggeler, R., Sagermann, M., and Capaldi, R. A. (1989) *Biochemistry 28*, 4717−4724.
43. Wilkens, S., and Capaldi, R. A. (1992) *Arch. Biochem. Biophys. 299*, 105−110.
44. Wilkens, S., and Capaldi, R. A. (1994) *Biol. Chem. Hoppe-Seyler 375*, 43−51.
45. Landolt-Marticorena, C., Kahr, W. H., Zawarinski, P., Correa, J., and Manolson, M. F. (1999) *J. Biol. Chem. 274*, 26057−26064.
46. Zhang, J., Vasileyeva, E., Feng, Y., and Forgac, M. (1995) *J. Biol. Chem. 270*, 15494−15500.

47. Bowman, E. J., Steinhardt, A., and Bowman, B. J. (1995) *Biochim. Biophys. Acta 1237*, 95−98.
48. Nelson, H., Mandiyan, S., and Nelson, N. (1995) *Proc. Natl. Acad. Sci. U.S.A. 92*, 497−501.
49. Boekema, E. J., Ubbink-Kok, T., Lolkema, J. S., Brisson, A., and Konings, W. N. (1997) *Proc. Natl. Acad. Sci. U.S.A. 94*, 14291−14293.
50. Wilkens, S., and Capaldi, R. A. (1998) *Nature 393*, 29.
51. Böttcher, B., Schwarz, L., and Gräber, P. (1998) *J. Mol. Biol. 281*, 757−762.
52. Karrasch, S., and Walker, J. E. (1999) *J. Mol. Biol. 290*, 379−384.
53. Adachi, I., Puopolo, K., Marques-Sterling, N., Arai, H., and Forgac, M. (1990) *J. Biol. Chem. 265*, 967−973.
54. Gräf, R., Lepier, A., Harvey, W. R., and Wieczorek, H. (1994) *J. Biol. Chem. 269*, 3767−3774.
55. Merril, C. R., Goldman, D., Sedman, S. A., and Ebert, M. H. (1981) *Science 211*, 1437−1438.
56. Carazo, J. M., Wagenknecht, T., Radermacher, M., Mandiyan, V., Boublik, M., and Frank, J. (1988) *J. Mol. Biol. 201*, 393−404.

BI000103U